Melanin thin-films: a perspective on optical and electrical properties

J.V. Paulin[a,b], A. P. Coleone[a], A. Batagin-Neto[a,c], G. Burwell[b], P. Meredith[b,d], C.F.O. Graeff[a,e], A.B. Mostert[f,*]

[a] São Paulo State University (UNESP), School of Sciences, Postgraduate Program in Science and Technology of Materials (POSMAT), Bauru, Brazil.

[b] Swansea University, Department of Physics, Singleton Park, Swansea, SA2 8PP, United Kingdom.

[c] São Paulo State University (UNESP), Campus of Itapeva, Itapeva, Brazil.

[d] School of Mathematics and Physics, University of Queensland, St Lucia Campus, Brisbane Queensland 4072, Australia.

[e] São Paulo State University (UNESP), School of Sciences, Department of Physics, Bauru, Brazil.

[f] Swansea University, Department of Chemistry, Singleton Park, Swansea, SA2 8PP, United Kingdom.

Corresponding author:
a.b.mostert@swansea.ac.uk (A.B. Mostert).

Abstract

Melanins are an essential natural pigment found throughout nature. Due to their inherent biocompatibility, optical and electronic properties, the melanins are attracting attention as model materials for sustainable organic optoelectronic and bioelectronic applications. Standard melanin is notoriously insoluble, which complicates processability considerably. Hence, the creation of synthetic derivatives that have similar optical-electronic properties but with increased solubility are avenues of active investigation. In this work, we investigate soluble non-functionalized (NF) and sulfonated (S) melanin derivatives. So far, these new synthetic derivatives' optical and electrical properties have not been explored in full, which would allow their effective application in optoelectronic devices. Our optical results suggest that these materials have a high refractive indices and also high dispersion and chromatic aberration. In addition, no significant differences in NF-melanin's charge transport deposited from pure water or aqueous ammonia solution were observed, and S-melanin's functional groups did not affect the hydration-dependence conductivity, only its sensitivity to environmental humidity. The similarities and differences in spectra and values comparing NF and S-melanin are discussed based on their structural differences.

Keywords: Melanin; melanin derivatives; optical properties; electrical properties; bioelectronic materials.

Introduction

The melanins are an important class of biological pigment found throughout nature.[1–3] These materials can be divided into different systems such as eumelanin, pheomelanin, neuromelanin and allomelanins, representing different molecular building blocks.[1–3] In the human body, melanins are believed to be involved in a variety of processes ranging from photoprotection, accumulation and release of metal ions,[4,5] radical scavenging,[6] antimicrobial behavior[7] and multifunctional antioxidant.[3,6] Paradoxically, they have also been implicated in melanoma skin cancer and neurodegenerative diseases like Parkinson's and Alzheimer's.[8] As a materials class, the melanins garner a growing interest from physicists, chemists and material scientists for potential applications in biomedical and technological settings, including surface coatings, nanomedicine, bioelectronics and sustainable organic optoelectronics. Particularly, melanins have been used in a series of common electronic components such as batteries,[9–12] capacitors,[13–16] light-emitting diodes,[17–19] memories,[20–23] photoelectrodes,[24] solar cells[11,12,25,26] and transistors.[27–30]

A central endeavor for modeling and design optimization for (bio)organic optoelectronics devices is the ability of producing homogeneous and smooth device-quality thin-films and accurately understanding their optical and electrical properties. In this regard, the most common category eumelanin (or, hereafter, termed melanin for simplicity[1]) has presented great difficulty due to its notorious insolubility.[1] From a practical technological perspective, using a high pH alkaline solution to disperse synthetic melanin is a straightforward approach.[31] Nonetheless, the high pH environment could induce structural alterations as a result of oxidative degradation.[3]

Since solubility is a key issue in processibility, a strategy is to make a highly soluble "*melanin*" that retain its other desirable material properties.[32–38] One approach to this end is to use positive oxygen pressures of the standard synthetic melanin procedure, which yields a water-soluble material with a slight higher oxidation state and a higher amount of carboxylic groups, implying a material with closer characteristics to natural melanin.[37] The water solubility is of great appeal since it could deliver efficient charge transport[36] in a biocompatible medium.

Another method to obtain soluble melanin-based materials is the introduction of an exotic functional group to the melanin structure. In such a case, the melanin precursor's oxidation in dimethylsulfoxide (DMSO) creates a sulfonated melanin. The presence of the sulfonated groups improves the solubility of sulfonated melanin in DMSO, *N*-Methyl-2-pyrrolidone (NMP) and *N,N*-dimethylformamide (DMF), but has been shown not to affect other interesting properties such as biocompatibility,[39] redox activity,[30,40] paramagnetism,[32,41] and, most importantly, the ability to

produce homogeneous and device-quality thin-films.[13,30,32,40,42] On top of that, the sulfonated groups' presence has allowed such derivatives to be easily deposited on both hydrophilic and hydrophobic surfaces, which amplifies their potential range for devices applications.

To understand the molecular engineering and the properties one would want to conserve, a brief overview of melanin's chemistry and properties is required by way of introduction. Synthetic melanin is a macromolecular system synthesized from two monomers, 5,6-dihydroxyindole (DHI) and 5,6-dihydroxyindole-2-carboxylic acid (DHICA) and their different redox states of hydroquinone (HQ), semiquinone (SQ), indolequinone (IQ) and quinone imine (QI) (see Figure 1(a)).[43] These monomers react to form small oligomers that then self-assemble in π–π-stacked supramolecular units of different sizes with an interplanar spacing of 3.7 Å.[1–3] This molecular system yields physicochemical properties like broadband UV-Vis absorbance[1] and stable free-radical structures,[1,44,45] biocompatibility[1] and hydration-dependence conductivity.[44,46–50] The underlying structure-property framework has been termed 'the structural disorder model' reflective of the diversity of molecular types, redox states, packing and assembly. Melanins' macroscopic properties are thus derived from ensemble averages over the structural disorder.

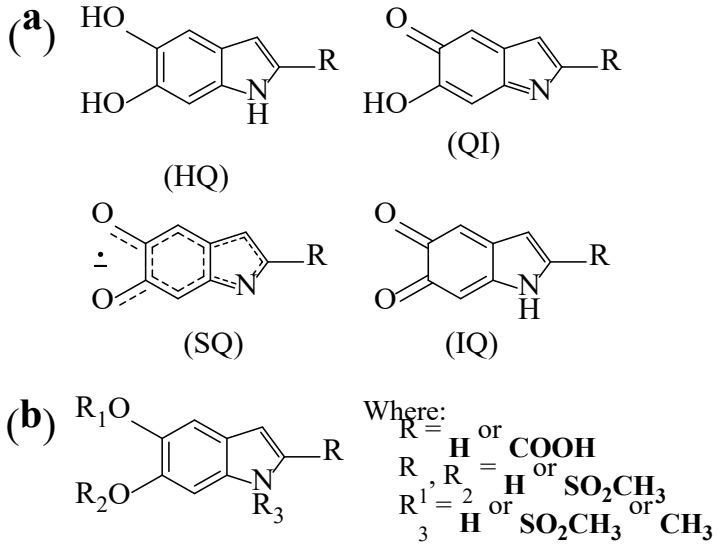

Figure 1. (a) The building block monomers of non-functionalized melanin. (b) Proposed building blocks of sulfonated melanins.[51] R = H (for DHI species) or R = COOH (for DHICA species).

The above-mentioned optical and conductive properties have been of interest for many years. The first is intimately linked by medical diagnostics,[52,53] UV-shielding[16,54] and as optical contrast in photoacoustic imaging;[55] the second by the aforementioned (bio)organic electronics applications. The electrical response of melanin is usually correlated with its redox

chemistry,[42,44,45,48–50,56] since the humidity level can modulate a chemical self-doping effect by releasing protons into the water matrix.[44] Such hydration-effect is of great importance due to its ability to change the conductivity by orders of magnitude.[44,46,49,57]

However, even with the significant advantages of the non-functionalized (NF-melanin) and sulfonated (S-melanin, Figure 1(b)) soluble derivatives, there has been no systematic study of their optical and electrical behavior. In fact, among these samples, only for sulfonated melanin there are a few reports about its electrical response from earlier conductivity as a function of temperature,[32] electrochemical measurements,[40] and some speculation from their free-radical property.[41] Hence, herein we report an extensive study on the optical and electric behavior of melanin's soluble derivatives. As a control, the standard (insoluble) synthetic melanin was used for comparison. Our results provide valuable information for melanin and melanin-like optoelectronics and bioelectronic device applications and extend the structure-property understanding in these important functional biomaterials.

Experimental

Non-functionalized melanin synthesis:[37,47]

5 g of 3,4-dihydroxyphenyl-DL-alanine (DL-DOPA; Sigma-Aldrich) was dissolved in 2 L of deionized water. Ammonia (NH_3; Sigma-Aldrich, 28 %) was used to adjust the mixture to pH 8. The solution was kept under constant stirred and with air bubbling for three days. After the third day, concentrated hydrochloric acid (Sigma-Aldrich, 25%) was used to adjust to pH 2 and precipitate the melanin. The aggregated solution was filtered, washed several times using deionized water, and dried overnight under ambient conditions to yield a black and insoluble powder (named NFMel-I).

0.3 g of DL-Dopa was dissolved in 60 mL of MiliQ water (18 MΩ cm). The mixture's pH was adjusted to be between 8 and 10 by the addition of 400 µL of ammonium hydroxide (NH_4OH; Synth, 28-30%). The solution was kept stirring at room temperature (~27ºC) and oxygenated using an air pump for three days (NFMel-S) or in a 150 mL stainless steel reactor with an internal pressure of 6 atm of industrial oxygen gas for 6 hours (NFMel-6P). After this period, the solution was placed in a 3500 MWCO dialysis membrane with MiliQ water as a dialysate medium for approximately four days. Finally, soluble black powders were obtained after drying the aggregated solutions in an oven at 90 °C for two days.

Sulfonated melanin synthesis:[32,33,38]

In 200 mL of DMSO (PA, Vetec, 99.9%), 1.50 g of DL-DOPA and 0.93 g of benzoyl peroxide (Vetec, 75.0-80.0 %) were dissolved in a flask. This mixture was kept under magnetic stirring for 58 days at room temperature (SMel) or eleven days in a temperature-controlled silicone bath at 100 °C with a reflux condenser attached to the flask (SMel-T). For extraction and purification, the reaction solution was concentrated to ¼ of the initial volume and then 150 mL of acetonitrile (Synth, 99.5%) was added to the concentrated solution. The new solution was allowed to stand for two days and, afterward, it was centrifuged at 2500 rpm for 15 minutes. The precipitate was dried in the oven at 90 °C for two days.

0.45 g of DL-DOPA was dissolved in 60 mL of DMSO. The solution was placed in a 150 mL stainless steel reactor and stirred with 4 atm of O_2 internal pressure for six days (SMel-4P) or 8 atm for three days (SMel-8P). The same extraction and purification procedure described for SMel and SMel-T was followed.

All commercial chemicals were used without further purification.

Melanin thin-films

Melanin thin-films were prepared by two-step spin-coating (500 rpm for 5 s and 2000 rpm for 60 s) with 30 mg/mL solution. The NF-melanin solutions were prepared by dissolving 30 mg of the respective sample in 1mL of a mixture of deionized water and ammonia (1 H_2O:2 NH_3 %v for NFMel-I or 3 H_2O:2 NH_3 %v for NFMel-S and NFMel-6P), stirred for 1 hour at 50 °C and then ultra-sonicated for 1 hour. After the sonication, the solution was filtered with a 0.45 μm Hydrophobic PTFE filter (Cole-Parmer). Additionally, S-melanin solutions were prepared by dissolving 30 mg of the sample in 1 mL of anhydrous DMSO (Sigma-Aldrich, ≥ 99.9%) or anhydrous NMP (Sigma-Aldrich, ≥ 99.5%) or anhydrous DMF (Sigma-Aldrich, ≥ 99.8%), stirred for 1 hour at 50°C and then filtered with a 0.45 μm Hydrophobic PTFE filter (Cole-Parmer).

The films were deposited onto two sets of substrates: glass slides (25 x 25 mm) for UV-Vis-NIR spectroscopy and silicon wafers (10 x 10 mm) for ellipsometry. The glass slides were initially cleaned with a soap solution (Alcanox®), rinsed in water; ultra-sonicated in acetone (15 min), followed by 2-propanol (15 min), and dried under a flow of nitrogen. The silicon wafers were cleaned similarly to the glass with a soap solution (Alcanox®) and rinsed in water, but they were ultrasonicated two times in acetone (10 min each), followed by two times in 2-propanol (10 min each) and dried under a flow of nitrogen. Both substrates were treated with UV-ozone (20 min)

prior to melanin deposition.

We also performed an elemental analysis of the samples via X-ray photoelectron spectroscopy to confirm the composition of the films. The data was obtained via an XPS wide-scan survey spectrum of the deposited films utilizing a Kratos Axis Supra using a 225 W AlKα X-rays with an emission current of 15 mA and equipped with a quartz crystal monochromator with a 500 mm Rowland circle. Spectra were collected with a pass energy of 40 eV, with the hybrid lens setting, 0.1 eV step size, 1 s dwell time for electron counting at each step. The integral Kratos charge neutralizer was used as an electron source to eliminate differential charging. As previously demonstrated. The atomic composition (atomic concentration in at% and atomic ratio) can be seen in Table S1. Surface scans of these melanins are representative of the bulk and the composition is compatible with melanin derivatives as previously demonstrated.[58]

Optical measurements

Transmission and reflectance spectra were obtained on standard glass slides using a 150 mm diameter integrating sphere coupled to a Lambda 950 UV-Vis-NIR spectrometer (Perkin-Elmer). A wavelength range between 2100 and 300 nm, a wavelength step of 5 nm, a scan rate of 5 nm at 923.6 nm/min and a slit width of 5 and 2 nm for PMT and InGaAs detectors were used. To evaluate if our films scatter, we have measured the normal transmittance in a standard mode and using an integrating sphere. The spectra showed in Figure S1 (in Support information) indicate that there are few differences between both setups, which indicates no significant scattering effect from our samples. Such behavior is compatible with earlier studies that showed that the optical properties of melanin are due to electronic nature, i.e., actual aborption.[31]

Ellipsometry measurements were taken with a J. A. Woollam M-2000 spectroscopic ellipsometer equipped with a xenon lamp source over a wavelength range of 370–1700 nm. Simulation analysis of the Variable Angle Spectroscopic Ellipsometry (VASE) experiment in 1 nm steps with incidence angles of 65°, 70°, and 75° relative to the surface normal was used to determine the optical constants using the CompleteEASE software (v. 5.23).

Electronic structure calculations

Distinct units of NF- and S-melanins were considered to estimate the refractive indices. The molecules were designed with the aid of the Molden computational package.[59] Molecular dynamics calculations at high temperature were conducted to identify the most stable structures, as reported

in ref [41]. All the conformers were pre-optimized in a Hartree−Fock approach using the PM6 semiempirical approximation as implemented in the MOPAC2016 computational package.[60] The most stable structures were selected and fully optimized in the framework of the density functional theory (DFT) using the B3LYP[61] hybrid exchange-correlation functional and 6-31G(d,p) basis set on all the atoms, with the aid of Gaussian 09 computational package.[62]

The refractive indices *n* of the molecules were theoretically predicted from the macroscopic optical susceptibilities,[63] χ, as follows:

$$n = \sqrt{1 + 4\pi\chi} \tag{1}$$

where,

$$\chi = \frac{N\,\alpha'}{1 - \left({}^{4\pi}/_{3}\right) N\,\alpha'} \tag{2}$$

$$N = \frac{\Gamma \cdot N_A \cdot \rho_m}{M} \tag{3}$$

$$\alpha' = \frac{\alpha_{iso}}{4\pi\varepsilon_0} \tag{4}$$

$$\alpha_{iso} = \frac{1}{3}\left(\alpha_{xx} + \alpha_{yy} + \alpha_{zz}\right) \tag{5}$$

N is the density of molecules, α' represents the volume of polarization, Γ is coefficient of 10^6, N_A is the Avogadro's constant, ρ_m the mass density, M the molar mass and ε_0 the vacuum permittivity. α_{iso} represents the polarization constant, which was estimated via DFT/B3LYP/6-31G(d) calculations.

Device fabrication and electrical measurements

Glass slides (10 mm x 10 mm) were cleaned with Alcanox®, rinsed in water, ultra-sonicated in acetone (15 min), 2-propanol (another 15 min), and dried under a flow of nitrogen. Then, 50 nm thick gold interdigitated electrodes with 100 μm length and 11.2 mm width channel was thermally evaporated. The electrodes were finally treated with UV-Ozone (5 min) and, soon after, melanin was spin-cast at 500 rpm for 5 s followed by 1500 rpm for 60 s. At least six different pairs of electrodes from two different substrates were used.

Humidity-dependent measurements were carried out using a JANIS Research Cryogen Free

Micromanipulator probe station attached to a steam delivery system (whose schematics is discussed in detail elsewhere[47]). The JANIS chamber was initially pumped down to vacuum (~10^{-2} mbar) overnight using a rotary pump to ensure that all samples were completely dried. Degassed water vapor was introduced sequentially into the system to obtain four hydration levels: 0, 40, 80, and 100 %. Since the material system is a mixed ionic/electronic conductor, a 4-point measurement would be counterproductive, because both ionic and electronic charge carriers can't be injected and extracted simultaneously at the contacts. Therefore, the current-voltage data were measured using a Keithley 2450 with two-point electrodes using a step voltage of 0.02 V. Consistent geometry and contacting electrode ensures at least a good relative comparison between materials and within a hydration curve. The voltage was swept forward and backward from -1 to 1 V to prevent electrochemical water splitting into hydrogen and oxygen, which occurs at a potential difference of 1.2 V, and reduced additional systematic uncertainty in the measurement. Electrical impedance spectroscopy was performed sweeping through a frequency range from 10^{-2} Hz to 10^{4} Hz only at the 100% hydration level with a two-electrode cell and Metrohm Autolab PGSTAT302N with FRA32M module. A sine wave, 0.1 V of amplitude and 10 frequencies per decade were used. EIS spectra were simulated using the ZView-impedance Software (v. 2.8d). The low voltage amplitude (with no DC bias) does not transgress previously published voltages for redox activity in either sulfonated melanins[40] or non-functionalized melanins.[64] Furthermore, our geometry and voltages (<0.2 V) would not induce redox activity as reported elsewhere, as supported by the lack of a 2nd, low frequency semicircle in our EIS data.[48] As such, the measurement does not induce redox activity and captures the electronic/ionic currents, as is the purpose of this work. However, future work aimed at elucidating the redox activity should include DC bias to EIS measurements.[48]

Atomic Force Microscopy characterization

Atomic force microscopy (AFM) was used to measure the surface morphologies of the films. A JPK NanoWizard II (Bruker) system was used in tapping mode with Sharp Nitride Lever (SNL-10, Bruker) probes. 5x5μm scans were obtained at three locations per sample. Data analysis was performed using Gwyddion[65] software; polynomial background and row alignment processes were used before extracting roughness parameters. 1x1μm regions were also selected away from larger features to obtain roughness parameters that were representative of the underlying film. Data is presented in the Supplementary Information.

Results and discussion

Optical properties

The transmittance and reflectance as a function of wavelength (λ) of each melanin derivative are displayed in Figure 2 (and Figures S2-S4). In most cases, it is possible to divide the transmittance spectra into three different regions. The first and the last one is dominated by the glass substrate ($\lambda_{Glass} < 350$ nm and $\lambda_{Glass} > 850$ nm), while the intermediate region is dominated by the melanin thin layer ($350 \geq \lambda_{Melanin} \leq 850$ nm). As shown in Figure 2(a, b), the melanin transmittance spectra show an exponential decay in the visible region with a sudden drop at high energies. Such behavior is related to a high absorbance in the ultraviolet and visible areas. Additionally, the NF-melanin films displayed high transmission at 500 nm, around 75.6% from alkaline solution (H_2O+NH_3) and 83.5% from a neutral solution (distilled water); whereas for S-melanin 82.8% from DMSO, 77.1% from DMF and 84.6% from NMP solutions. Furthermore, reflectance lower than 15% was obtained for all samples Figure 2(c, d). We note that the films did not suffer any eye-distinguishable brown colored changes (Figure S5), which implies that the intensity differences for both transmittance and reflectance are most likely due to film thickness variations.

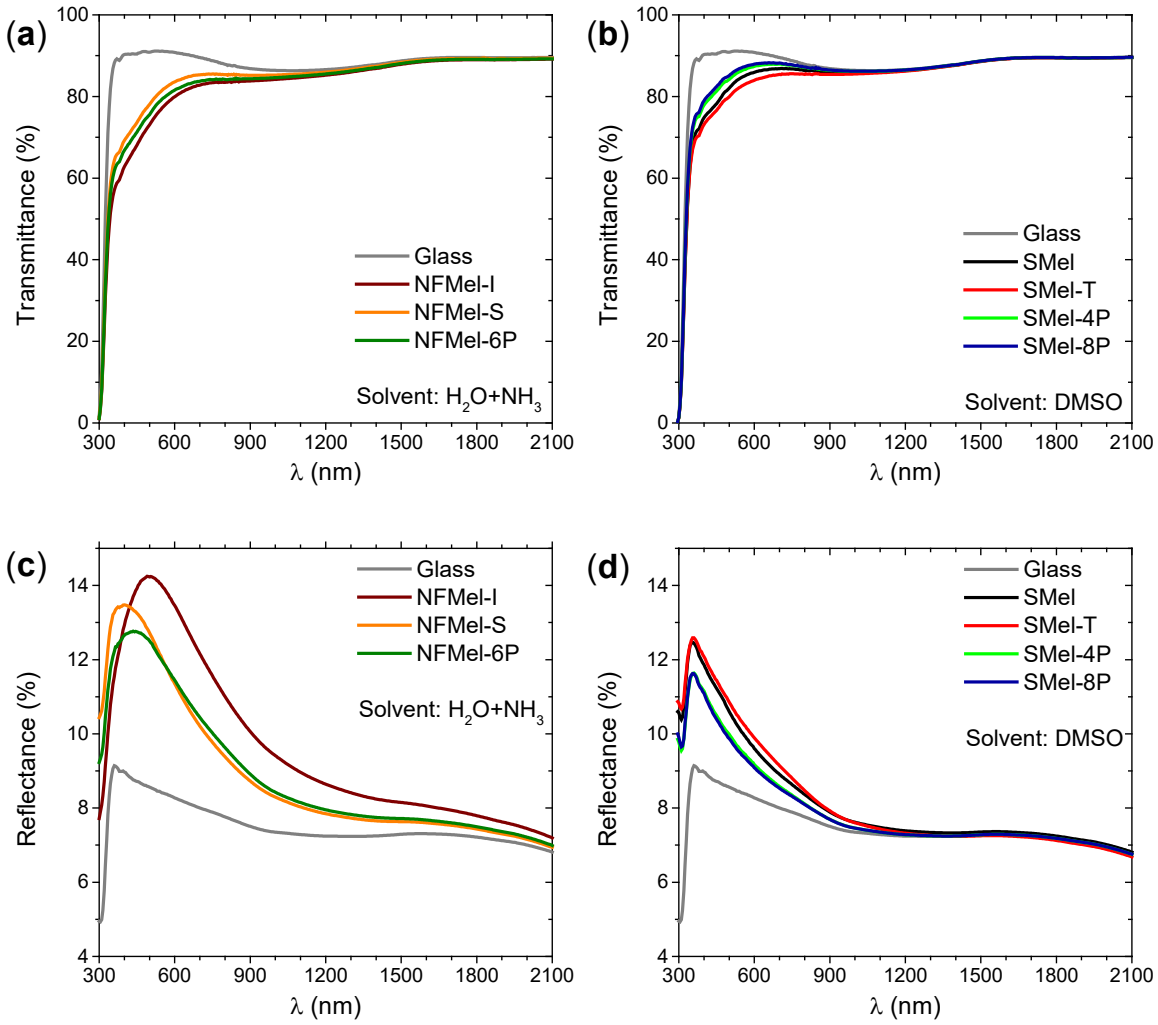

Figure 2. Transmittance (a, b) and reflectance (c, d) spectra of NF-melanin (a, c) and S-melanin (b, d). Similar features can be observed for other solvents.

The absorbance can be calculated from a simple relation of the transmittance and reflectance spectra, A = 1 – T – R, assuming that the optical scattering is negligible. As shown in Figure S1, the scattering of our films is negligible, again indicative of high-quality thin films. Hence, the above relation is valid to calculate the absorbance. Their values were normalized by the film thickness (estimated from the optical transmission spectra[66]) are shown in Figure 3 and Figures S6-S7. This also highlights, that even for some films exhibiting small particles on the surface (Figures S8-S11 and Table S2), which may act as scatterers, they did not do so and as such the absorbance is most likely due to the bulk film. As can also be seen, there is no essential change in the qualitative behavior between both sample groups; that is, the absorbance spectra exhibit a featureless decaying response as a function of increasing wavelength. However, it is possible to

note that there are quantitative differences in intensity. This could indicate that in sulfonated melanin derivatives, the light-absorbing chemical moieties are present in smaller quantities than non-functionalized ones. Usually, melanin chromophores can be defined by the conjugation length of absorbing species and different oxidized and reduced chromophores units.[35,67] Therefore, the optical absorbance differences can reflect the differences in oligomeric structures due to the presence of the sulfonated groups. Melanins also tend to aggregate, reducing solubility and increasing light absorbance and dispersion.[68] Hence, S-melanin's lower absorbance and better solubility compared to NF-melanin could be partially explained if one considers that the first is composed of smaller structures with a low degree of aggregation, as shown in earlier studies,[13,42,69] probably due to the sterical hindrance of the sulfonated group. Future studies with small-angle neutron scattering and small-angle X-ray scattering will be essential to understand in full its macrostructure. Also, it has been proposed that the functionalization occurs at the hydroxyl group of indole monomeric structure,[51] which could, by itself, perturb the interactions between the oxidized and reduced moieties in the polymer chain, affecting its optical response.

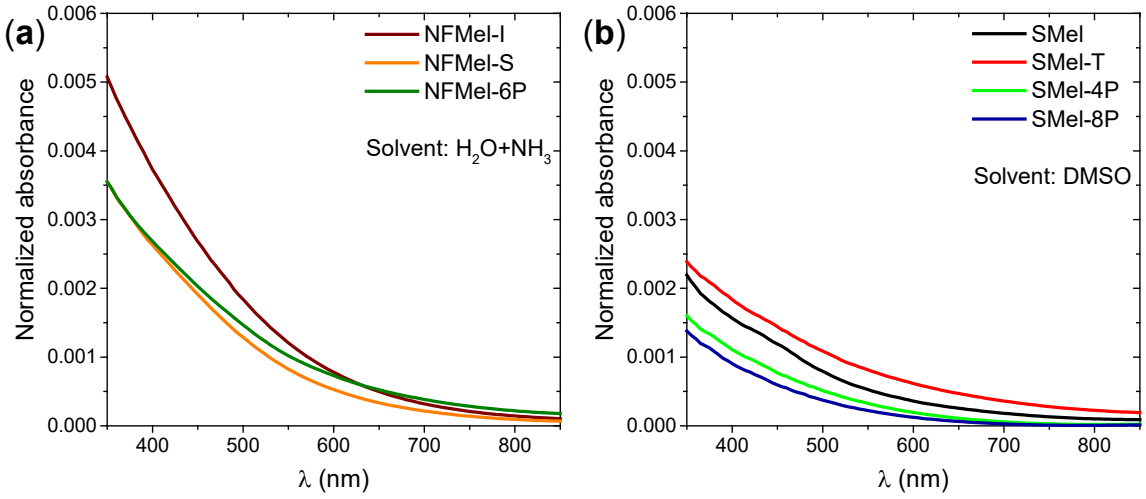

Figure 3. Calculated absorbance spectra normalized by the film thickness of NF-melanin and S-melanin. Similar behavior was found for NFMel-S & NFMel-6P in pure water and S-melanin in NMP and DMF solutions.

As mentioned in the Introduction, melanins are used as model materials for biocompatible optoelectronic applications, which means that other important properties to study are the optical constants, i.e., extinction coefficient (*k*) and refractive index (*n*). Figure 4 shows the VASE spectra and the optical constant for thin-films of NFMel-I in H_2O+NH_3 and SMel-T in DMSO. A three-

layer model was employed to fit the ellipsometry parameters $\Delta(\lambda)$ (delta) and $\Psi(\lambda)$ (psi): i) polycrystalline silicon as substrate, ii) native silicon oxide, and iii) a homogeneous synthetic melanin coating. Considering that melanin is a high-absorbing and amorphous material, a multi oscillator Tauc-Lorentz dispersion model was used to determine its optical properties.[70] We have also tried to use a single-layer Bruggeman effective medium approximation to account for any additional roughness of the melanin layer; however, no improvements in the fit were obtained. Therefore, to avoid over parameterization, we constrained our fit with only three layers.

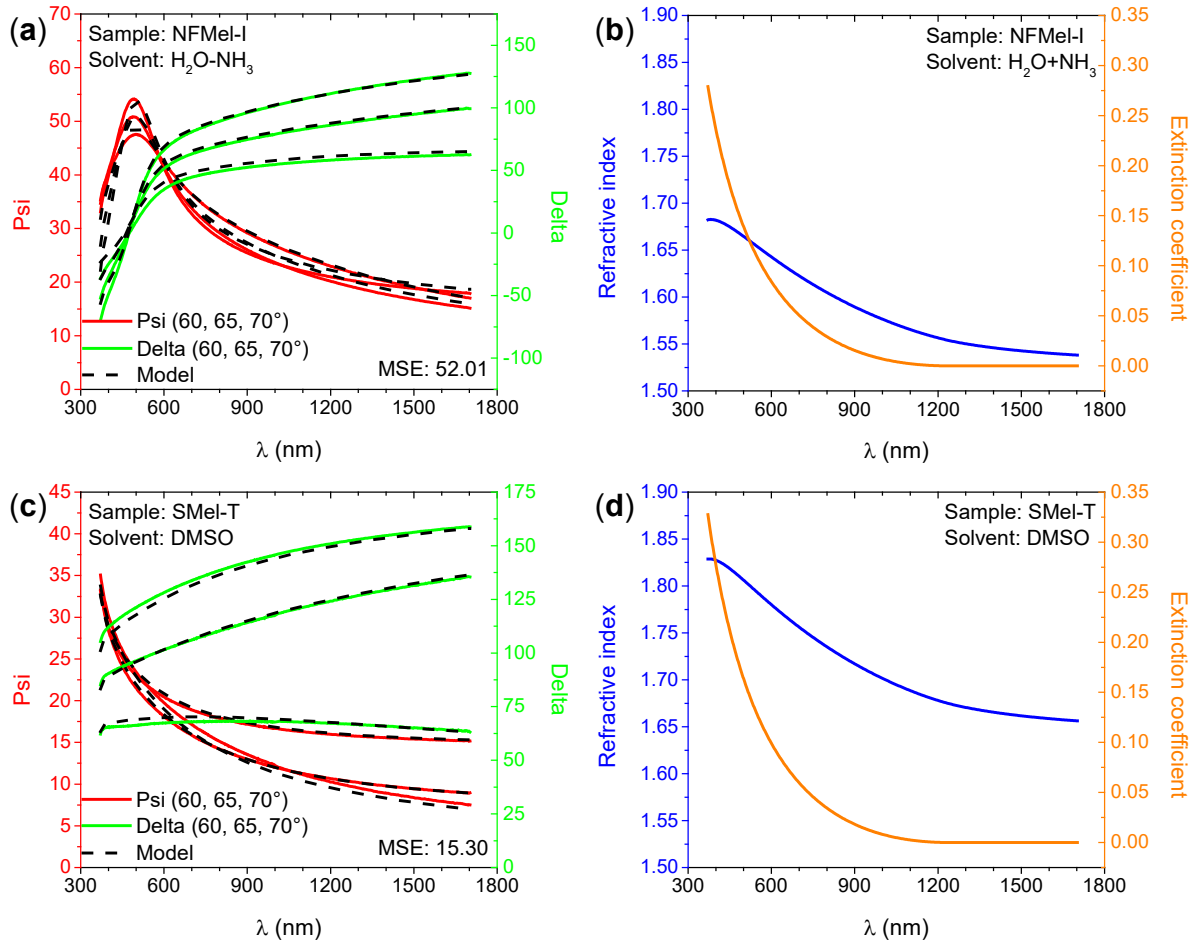

Figure 4. VASE spectra (a, c) and optical constants (b, d) of NFMel-I in H_2O+NH_3 (a, b) and SMel-T in DMSO (c, d). Similar behavior was obtained for the other samples, but with different intensities (Figure S12).

From the extinction coefficient, we have calculated the absorption coefficient (α) using the relation $\alpha = \frac{4\pi k}{\lambda}$. The melanin's absorption behavior increases with the wavelength (Figure S13)

and it is in line with solution measurements.[33,38] The refractive indices of NF and S-melanin increase towards higher energies[70,71] and despite presenting a similar form, the spectra have shown different magnitudes with no observed pattern (Figure S12). To obtain the refractive index of each melanin derivative, *n(λ)* was fitted to the Cauchy equation, $n(\lambda) = n_{Cauch} + \xi_{Cauch}\,\lambda^{-2}$, where ξ_{Cauch} is a proportionality factor.[66,71] The n_{Cauch} (for $\lambda \rightarrow \infty$) *of* all samples is summarized in Figure 5.

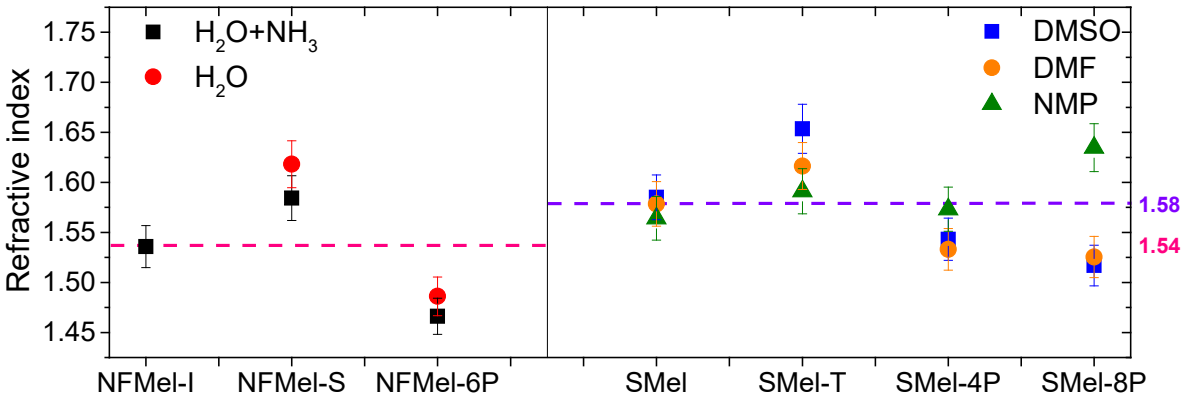

Figure 5. Refractive index values, following $\boldsymbol{n(\lambda) = n_{Cauch} + \xi_{Cauch}\,\lambda^{-2}}$ with $\lambda \rightarrow \infty$, for NF- and S-melanin. The left side legend indicates the refractive index scale; whereas the right side, the average value of the refractive index for NF-melanin (1.54 ± 0.06) and S-melanin (1.58 ± 0.04), represented by the pink- and violet-colored dashed lines.

The relative invariance of the refractive indices between the different melanin derivatives was unexpected due to the sulfur atom's well-known ability to increase *n* of many other materials.[72,73] It is known that high packing density materials can have high-*n* values ($n > 1.5$),[72,74] which implies that NF-melanin can intrinsically be a material with high-*n*. On this basis, the lower packing propensity of S-melanin[38] could decrease its refractive index. Accordingly, the combination of low packing density and the presence of the sulfur atom of S-melanin should be responsible for the equivalence in the refractive indices of both groups of samples.

Figure 6 displays the theoretical calculation performed to obtain further insights regarding the refractive index values for each possible monomeric species (see Figure S14). As can be noticed, the *n* values of the different monomeric species do not show significant variations, being compatible with the estimated experimental values; however, S-units tend to be slightly higher. Therefore, the theoretical calculations indicate that the similarities between NF and S-melanin

could also be explained, in the case of the latter, by the heterogeneous system composed of both NF and S moieties.[41]

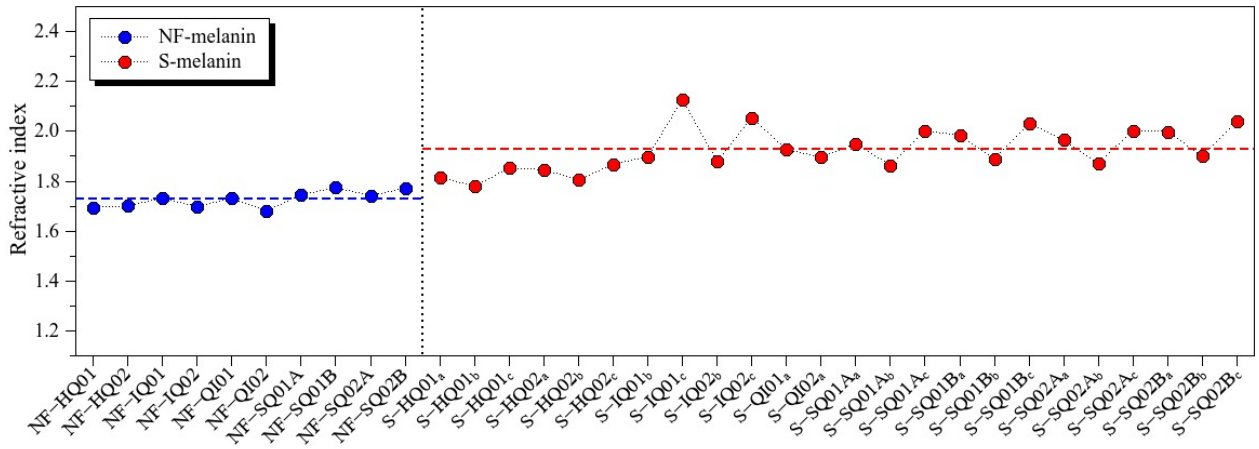

Figure 6. Refractive indices based on static susceptibilities (at $\lambda \rightarrow \infty$) of melanin units. The dashed lines represent the average values: 1.727 and 1.927 for NF and S-units, respectively. 01 number refers to DHI units, whereas 02 to DHICA units (see details in Figure S14).

Another important parameter for optical applications is the optical dispersion of a material in the visible region.[72,74] The optical dispersion is evaluated using Abbe's number (υ_D)[72,74,75] and it is determined by $\upsilon_D = (n_G - 1)\cdot(n_B - n_R)^{-1}$, where n_B, n_G, and n_R are refractive indices of the material at the wavelengths of the three primary colors (blue at 486 nm, green at 589 nm and red at 656 nm). Both NF and S-melanin derivatives displayed a low Abbe's number (17.86 ± 0.14, see Table S3), implying that the melanin films will present higher dispersion and higher chromatic aberration, when compared to other standard materials as poly-methyl-methacrylate ($\upsilon_D = 57$) and polystyrene ($\upsilon_D = 30$),[75] which would limit their use for photonic devices. However, note that for applications where high absorption material is needed, melanin would still be a great candidate.

Electrical properties

DC and AC measurements were performed to study the several soluble melanin derivatives' charge transport properties and compare them to the standard melanin (NFMel-I). Figure 7 presents the current *vs.* voltage curves as a function of hydration level for NFMel-I in H_2O-NH_3 (a) and SMel-T in DMSO (b). The behavior observed for these two samples are excellent representatives for the other non-functionalized (Figure S15 & S16) and sulfonated (Figure S17) derivatives. Also, we focus on sulfonated melanins processed with DMSO since these materials yielded the highest

currents at ambient pressures (Figure S18). An additional note, since the samples are bottom contacted, the measurements would go through the bulk of the material and avoid any surface aggregation effects as seen on some films via AFM (Figures S8-S11).

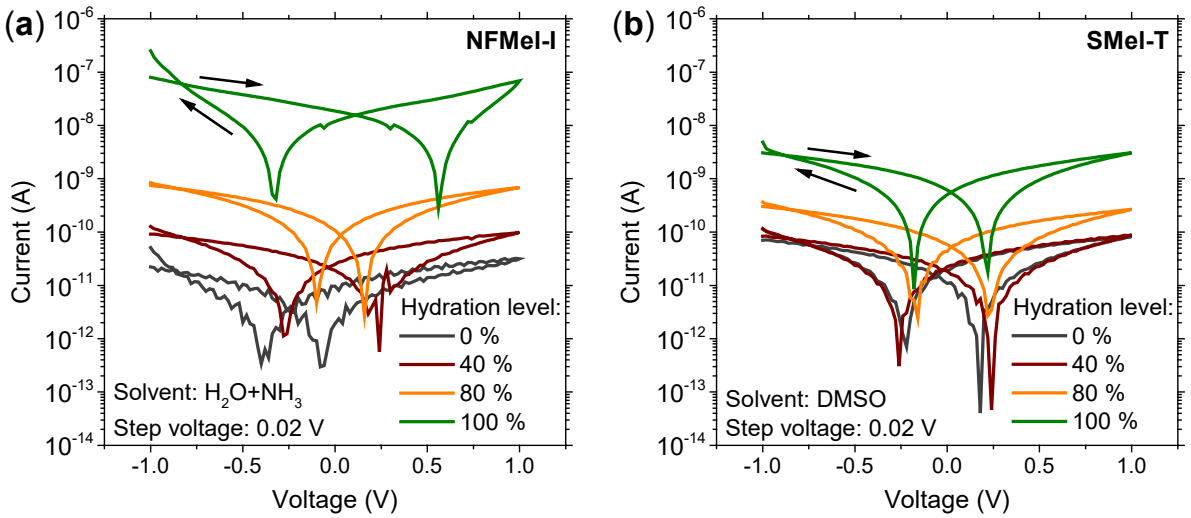

Figure 7. Current as a function of voltage for (a) NFMel-I in H_2O-NH_3 and (b) SMel-T in DMSO at different hydration levels on a log-linear scale. Note that the peaks in the curves are an artifact of taking the modulus of the positive and negative current values to enable a log-linear plot, and as such are not redox potential peaks. Each IV curve is an average of at least six different samples. Similar behaviors were found for other samples.

From Figure 7, it is clear that for both groups of samples, the current increases as a function of hydration, which could be understood as a rise in charge carrier concentration, protonic and electronic, due to the interaction between fully reduced (HQ) and fully oxidize (IQ) units in the presence of water to form semiquinones (SQ) and protons (H^+), following the comproportionation equilibrium reaction ($HQ + IQ + 2H_2O \rightleftarrows 2H_3O^+ + 2SQ$). Figure 7 also shows a hysteresis between the forward and backward sweeps, most likely linked to the protonic species' capacitive and space charge effects since they would be slow-moving, and unable to be extracted at the gold electrodes. However, one may see that S-melanin has a lower sensitivity towards hydration, resulting from the lower interaction of its microstructure with water molecules.[41] Also, if one considers that DMSO's boiling point is approximately 190 °C, it could be that traces of the solvent molecules were still present even after the vacuum step. Hence, it could be that DMSO residues could compete with the water, hindering S-melanin's hydration behavior. However, considering the harsh nature of an active vacuum and the deliberate reintroduction of water at high concentrations, this latter scenario

is less likely.

With this IV data, it was possible to calculate the conductivity as a function of hydration and the results can be seen in Figure 8. The data reported in Figure 8 is the first of its kind for soluble derivatives of melanin.

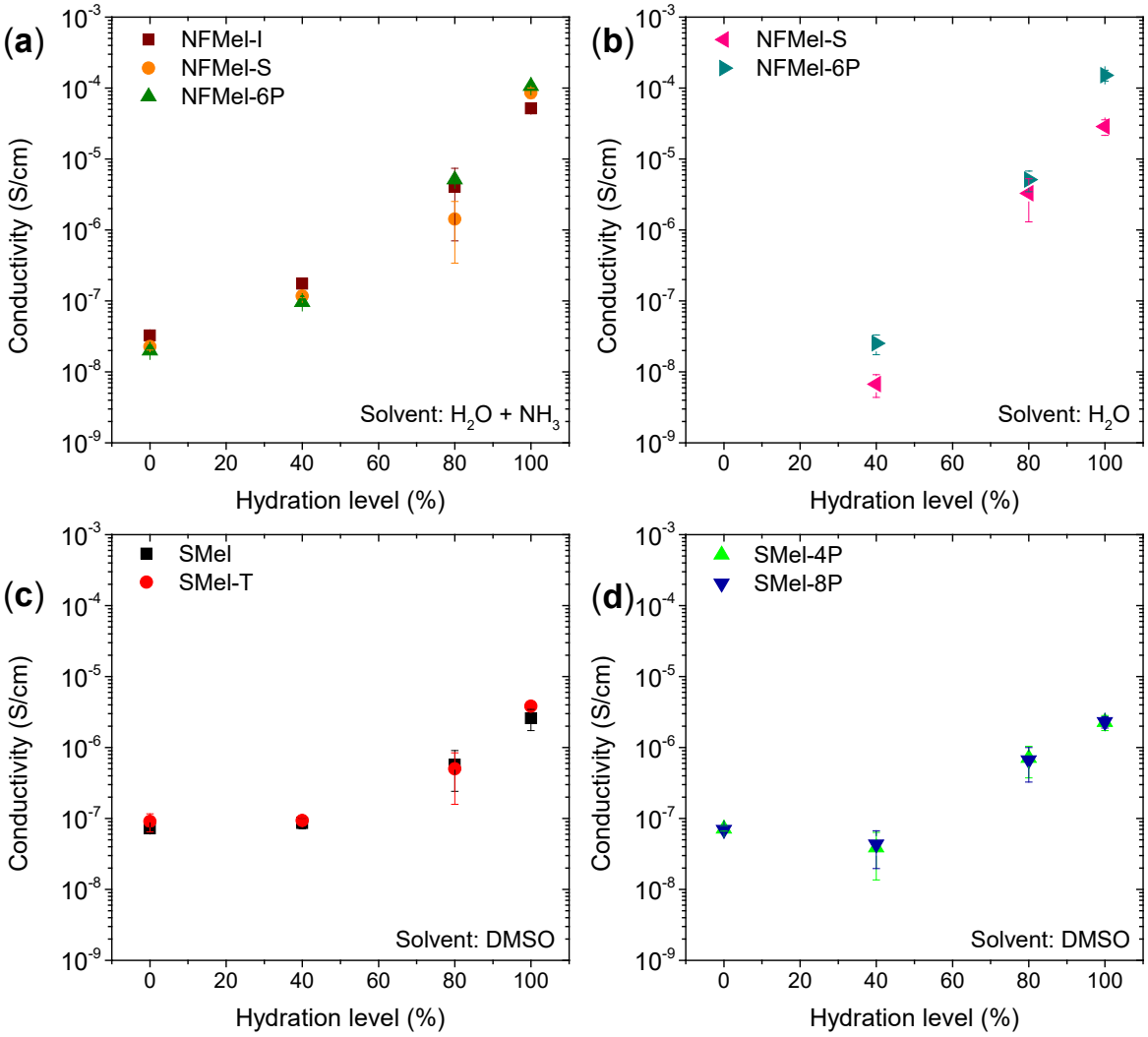

Figure 8. (a, b) NF-melanin and (c, d) S-melanin conductivity as a hydration function.

Figure 8 (a, b) shows, for the films prepared with H_2O+NH_3 solution, a range between 10^{-8} to 10^{-4} S/cm conductivity from 0 to 100% humidity is observed. On the other hand, from 40 to 100% humidity, films spin-coated from water only resulted in a variation of 10^{-9} to 10^{-4} S/cm. Note here that we could not calculate these samples' dry conductivities due to a dominant capacitive effect. The increase of the conductivity with hydration demonstrates that the ionic component has as expected a significant role in charge transport, as will be further elaborated with the AC data

below. Our result suggests that the ammonia's oxidation environment could assist in the deposition process and induce changes in the aromaticity of the samples and enhance its sensitivity to hydration. One possibility would be that the ammonia de-stack NF-melanin sheets, resulting in a higher surface area for melanin and water interaction. A similar assumption could also be verified by a slight increase in the conductivity of NFMel-6P compared to NFMel-S in both cases. It is known that NFMel-6P is composed of smaller particles,[37] which could lead to easy pathways for the water molecules to permeate through its macrostructure.

In addition, it was found that S-melanin's conductivity varies from 10^{-8} to 10^{-6} S/cm across the whole hydration scale, Figure 8 (c, d). The lower hysteresis, Figure 7 and Table S4, and the lower conductivity, Figure 8, of S-melanin derivatives could be partially explained by the lower S-macrostructure interaction with water.[41] The reduced interaction with water for the same hydration level would tend to indicate less ability to solvate protons than NF-melanin. So, if there are fewer protons available due to the presence of the sulfonate groups at the indole ring's hydroxyl group, and less water means less ability to solvate, these together will undoubtedly give a lower conductivity.

Another interesting feature comparing both groups of samples at 100% hydration is that the IV curve of S-melanin still shows an ohmic behavior, which is not the case of NF-melanin (see Figure 7 and Figure S19). The non-ideal current *vs.* voltage characteristic can be considered a signature of ionic (and protonic) transport,[76,77] corroborating our assumption that NF-melanin has a higher concentration of mobile ions than its S-counterpart.

In an attempt to investigate the charge transport dynamics of NF and S-melanins', we also employed electrochemical impedance spectroscopy (EIS) at 100% hydration level. Nyquist plots are displayed in Figure 9 for NFMel-I and SMel-T, as examples, and similar behaviors were obtained for the other samples (see Figure S20-S22). The imaginary *vs.* real components of the complex impedance exhibited a semicircle coupled to an upward nearly-linear line (or tail) at lower frequencies. Hence, we have modeled our data with a Randles circuit, schematically reported in Figure S23. We note that the Randles circuit has multiple interpretations, with the most common for electrochemical reactions being that there is a bulk solution resistance, a charge transfer reaction current and Warburg element that captures ionic diffusion near the electrode.[78] However, we interpret our data differently and choose an "ionic current" view in line with previously published work, since: 1) our sample is a solid-state electrolyte between two metal electrodes and as a result the low frequency tails we observe (see below) is due to electronic and ionic blocking

electrodes;[48,49,77] 2) that the voltage employed in the experiment is not enough to induce redox activity (<0.2 V) (see also methods section), which leads to 3) a lack of a 2nd low frequency semicircle indicating induced redox activity.[48] As such the elements we employ represent a resistor for the contact resistance, a second resistor to account for the ionic dissipation current, and the Warburg element associated with the diffusion of electroactive species at the blocking electrode surface, and a constant phase element (CPE) to represent surface modification capacitance and a dielectric double-layer.[77,79]

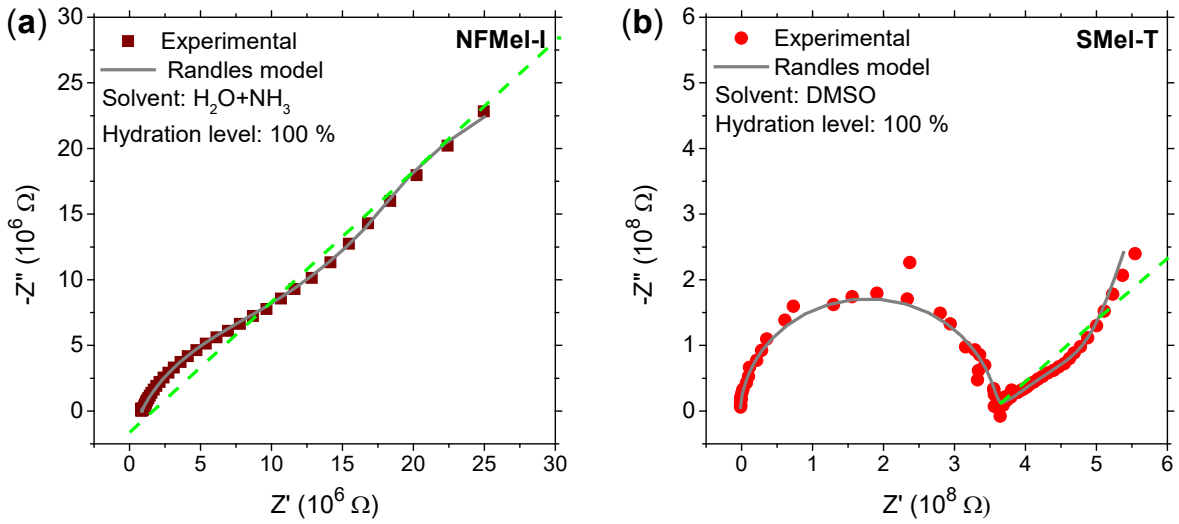

Figure 9. Nyquist plots from EIS measurements on (a) NFMel-I and (b) SMel-T at 100% hydration level. Scatter colored plots represent experimental data, while continuous gray lines the fit using the Randles circuit as a model. Dashed green line is set at 45°.

The complex impedance of CPE (Z_{CPE}) can be defined by $Z_{CPE} = [Q \cdot (j\,\omega)^{\eta}]^{-1}$, where j is the imaginary unity $(\sqrt{-1})$ and Q and η are fitting parameters, with $0 \leq \eta \leq 1$ [79]. For $\eta = 0$, CPE acts as a pure resistor; and for $\eta = 1$ as a pure capacitor. Based on our modeling, we have found $\eta = 0.78 \pm 0.08$ for NF-melanin and $\eta = 0.97 \pm 0.02$ for S-melanin (Table S5), in line with melanin and melanin-like materials ranging from 0.8 to 1 reported in literature.[27,80–82] These values imply that the CPE acts more like a capacitor. The observed differences could be an indication of the different transport mechanisms in the AC regime. In fact, the Nyquist plot (Figure 9) of NF-melanin is almost a straight line with ~ 45° slope over most of the frequency range, whereas, for S-melanin, there is a clear separation of a semicircle at high frequencies and the Warburg tail at low frequencies. Considering that usually the semicircle is related to the response of the bulk material and the straight line to diffusion processes at the vicinity of the interface with the

contact,[83,84] the different experimental shapes suggest that NF-melanin has an overlap between the frequency ranges of the two processes and S-melanin two distinct processes. Furthermore, Figure 9 shows that the linear tail is more pronounced for NF-melanin than S-melanin, indicating ionic domination in the first group sample. This idea is further corroborated with our hysteresis estimation that shows about two to three orders of magnitude difference (Table S4).

For a better comparison of the charge transport mechanism, we analyze the impedance modulus and phase angle as a function of frequency in Figure 10 for NF-melanin and Figure 11 for sulfonated derivatives. Figure 10 (a, b) shows, in the high-frequency region (f > 100 Hz), the impedance response of all samples is governed by a frequency-independent electronic process, which is compatible with the low phase angle in Figure 10 (c, d);[85] however, the peaks in the low-frequency domain (f < 100 Hz), ionic species diffusion takes place and controls the system response. The phase angle variation at the low frequency can suggest capacitive double layer formation,[85] a consistent interpretation observed elsewhere.[48]

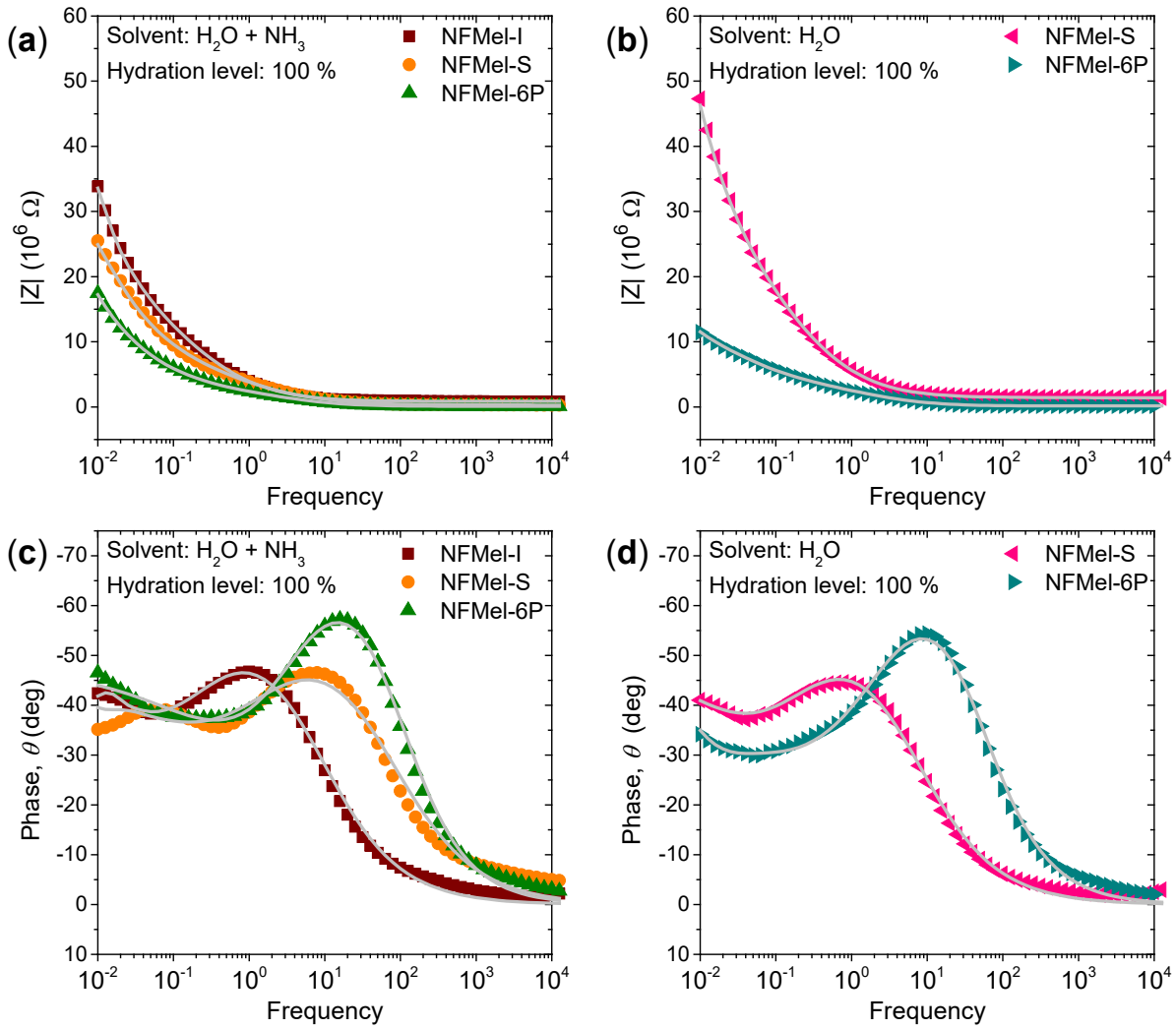

Figure 10. (a, b) Modulus and (c, d) phase angle as a function of frequency for NF-melanin films prepared using (a, c) water & ammonia and (b, d) water solution. Scatter colored plots represent experimental data, while continuous light gray lines the theoretical fit using a Randles circuit as a model.

The overall similarities between the three NF-samples indicate that the different methodologies used for film deposition provide only subtle changes to the charge transport, which legitimate the use of ammonia for film deposition. Most of all, the ionic component could be a consequence of small alterations in their macrostructures. When one compares the three samples in Figure 10(a, b), it is possible to observe a slight decrease in the NFMel-6P samples at the low-frequency domain. Considering that in the low-frequency region, ions dominate impedance, it is possible to speculate that the small impedance would be the consequence of an increase in the ionic conductivity, as indeed expected for a higher concentration of COOH in such sample.[37] If we

estimate the ionic conductivity of the semicircle diameter of the Nyquist plot at 100% hydration,[48,86] we obtain values of 7.6, 16 and 30 $mS \cdot cm^{-1}$ for NFMel-I, NFMel-S and NFMel-6P, respectively, in H_2O+NH_3 and 4.7 $mS \cdot cm^{-1}$ for NFMel-S and 31 $mS \cdot cm^{-1}$ NFMel-6P in only H_2O. These ionic conductivities are compatible with our previous discussion and the values reported in the literature for standard melanin[48,49] and other proton-conducting materials.[86,87]

Additionally, we note that there are significant differences in the impedance of NFMel-S when comparing the solution using an oxidizing (as in H_2O+NH_3 solvent) or neutral (deionized H_2O only) environment; however, none for NFMel-6P. Such absence of an effect from ammonia would be compatible with our earlier discussion about its impact on the melanin macrostructure. Considering that NFMel-6P has smaller particles than NFMel-S,[37] any structural variation caused by ammonia will not be significant enough to further increase its ionic conductivity. Note that the lack of a need to use ammonia for NFMel-6P can make it even more attractive for bioelectronic applications since we can overcome ammonia's genotoxic effects.[88]

By contrast, if one compares Figure 10 and Figure 11, the differences between the charge transport behavior of S and NF-melanin are evident. In the low-frequency domain of S-melanin, it is possible to see a subtle decrease in the impedance modulus until it reaches $f > 100$ Hz, see Figure 11(a, b), when the impedance drops. This result could indicate that S-melanin has mobile ions in lower concentrations (as discussed above) and, consequently, lower ionic conductivity. Indeed, in these samples, the estimated ionic conductivity was 0.2, 0.4, 0.2 and 0.1 $mS \cdot cm^{-1}$ for SMel, SMel-T, SMel-4P, and SMel-8P, respectively. However, the change in the impedance modulus at high-frequency could imply a preference for electronic charge transport. Note that the variation of impedance is more visible for samples synthesized with oxygen (SMel-4P and SMel-8P), suggesting that the different polymerization structures[38] result in a higher impedance, probably due to conjugation break. The angle phase, Figure 11(c, d), also supports the speculated mechanism since the variation in the high-frequency domain is more significant than in the low-frequency region. However, note that the phase is not zero at low frequency, implying that S-melanin also supports a lower ionic current.

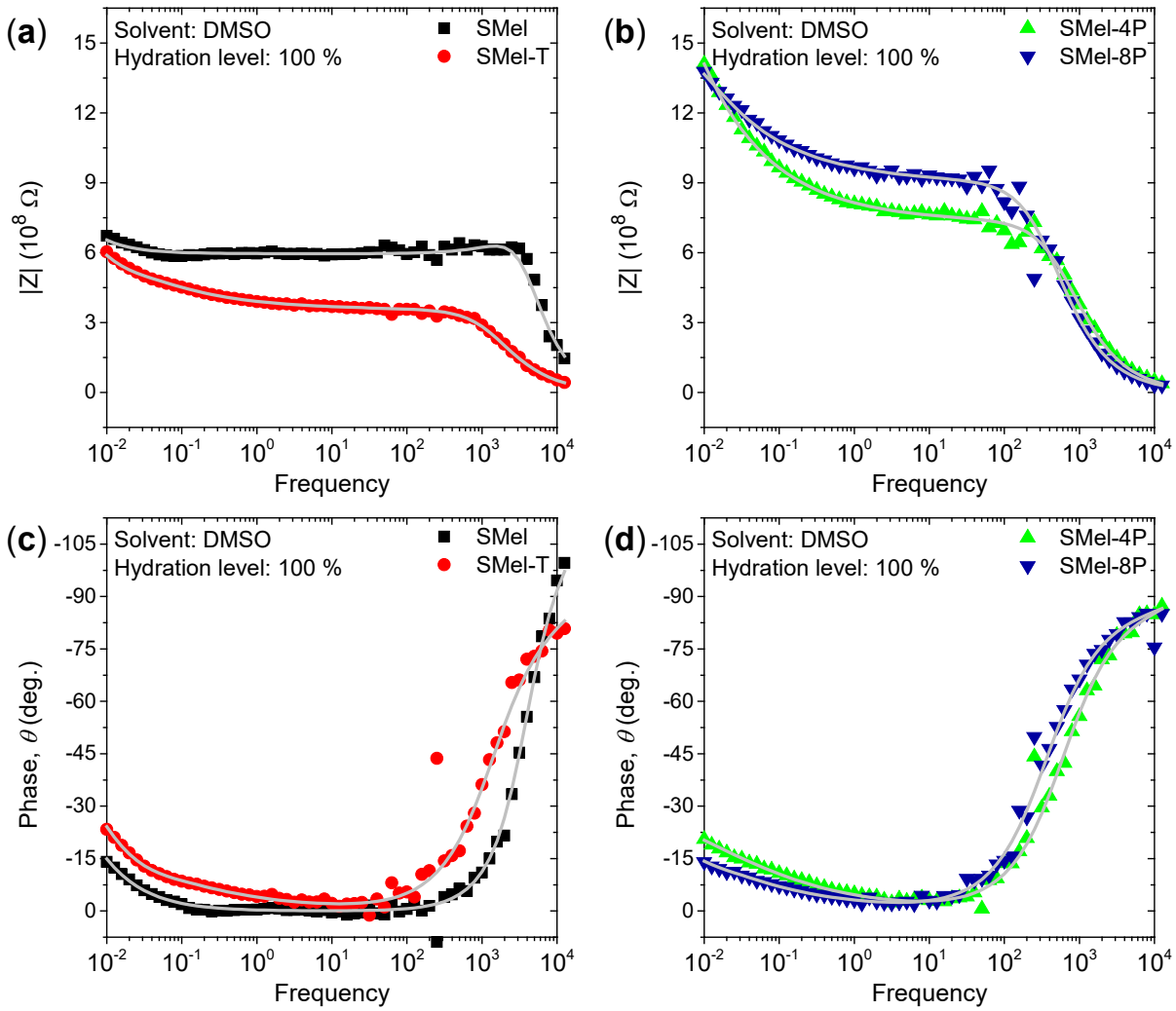

Figure 11. (a, b) Modulus and (c, d) phase angle as a function of frequency for S-melanin films prepared using DMSO solution. Scatter colored plots represent experimental data, while continuous light gray lines the theoretical fit using a Randles circuit as a model.

Given these observations, we speculate on the potential consequences for devices that can be based upon the S-melanins. S-melanins have many of the same redox moieties as standard melanin,[30,40,41] and that they do exhibit pseudo capacitance behavior,[40] they should be a prime candidate for supercapacitive behavior as work on NF-melanins reported by Kumar *et al.*.[15] However, given the lower protonic currents, they may not hold as much charge as a standard melanin. This aforementioned reasoning can also be extended to organic electrochemical transistors based upon melanin,[29] where they should function very well, but with an attenuated performance. However, given the higher parity between electronic and ionic charges, S-melanin may be an excellent candidate for more neuromorphic device applications.[89]

In summary, the above-presented results suggest that S-melanin derivatives have a lower ionic current with a potential enhancement in the electronic signal compared to NF-melanin. Both systems share similarities in their optical and electrochemical[30,40] properties. Overall, the S-melanins open exciting opportunities for device applications. Moreover, our findings could also assist further chemical engineering to tune the electronic properties of synthetic melanin derivatives.

Conclusions

We have conducted a detailed study of the optical and electrical properties of soluble melanin derivative thin films. The results show that the optical characteristics of sulfonated melanin behave similarly to non-functionalized melanins. For example, our films displayed high transmittance, high-*n* values, and low Abbe's number, which can potentially limit their use for photonics applications, where low absorption material is needed. The similarities in spectra and values comparing NF and S-melanin were discussed based on the structural differences.

The charge transport of the melanin thin-films was evaluated using DC and AC electrical measurements. Our results show no drastic changes in NF-melanin samples' electrical behavior using an alkaline solution (or not) to deposit the films. For S-melanin, the electrical conductivity proved to be hydration dependent, i.e., it increases with the water content, but with less variation than the NF counterpart. Such a result indicates that, even with the functional groups' presence, the S-melanin has active sites to facilitate mobile ions. An analysis of impedance measurements demonstrated that the sulfonated group decreases the S-melanin's ionic conductivity, but it may favor electronic processes at high hydration.

All these findings are an essential step towards developing bioelectronic and optoelectronic devices based on melanin, especially in the case of sulfonated derivatives with enhanced solubility.

Contributions

J.V.P. synthesized the materials and fabricated the devices. Optical and electrical data was obtained by J.V.P. with associated analysis. J.V.P. and J.D.M. obtained the XPS data. G.B. obtained the AFM and did the associated analysis. A.B.N. and A.P.C. performed the computational work. C.F.O.G., P.M. and A.B.M. conceived the original work. A.B.M. was responsible for overseeing the work. All authors contributed to the manuscript.

Acknowledgment

J.V.P., A.B.N. and C.F.O.G. gratefully acknowledge the financial support of São Paulo Research Foundation (FAPESP; grants 2012/03116-7, 2013/07296-2, 2015/23000-1, 2018/02411-1), National Council for Scientific and Technological Development (CNPq, grants: 573636/2008-7, 308360/2018-4, 420449/2018-3), Coordination for the Improvement of Higher Education Personnel (CAPES). P.M. is a Sêr Cymru II National Research Chair, which is supported by the Welsh Government through the European Regional Development Fund and an Honorary Professor at the University of Queensland. A.B.M. is a Sêr Cymru II fellow and the results incorporated in this work is supported by the Welsh Government through the European Union's Horizon 2020 research and innovation program under the Marie Skłodowska-Curie grant agreement No 663830. G.B.'s is supported by the Welsh Government's Sêr Cymru II Capacity Builder Accelerator Program through the European Regional Development Fund, Welsh European Funding Office, and Swansea University Strategic Initiative in Sustainable Advanced Materials. We also thank Dr. J.D. McGettrick, Swansea University, for helping obtain the XPS data.

References

1 P. Meredith and T. Sarna, *Pigment cell Res.*, 2006, **19**, 572–94.

2 S. Ito, K. Wakamatsu, M. D'ischia, A. Napolitano and A. Pezzella, in *Melanins and Melanosomes*, Wiley-VCH Verlag GmbH & Co. KGaA, Weinheim, Germany, 2011, pp. 167–185.

3 M. D'Ischia, K. Wakamatsu, A. Napolitano, S. Briganti, J.-C. Garcia-Borron, D. Kovacs, P. Meredith, A. Pezzella, M. Picardo, T. Sarna, J. D. Simon and S. Ito, *Pigment Cell Melanoma Res.*, 2013, **26**, 616–633.

4 L. Hong and J. D. Simon, *J. Phys. Chem. B*, 2007, **111**, 7938–7947.

5 A. B. Mostert, S. Rienecker, M. Sheliakina, P. Zierep, G. R. Hanson, J. R. Harmer, G. Schenk and P. Meredith, *J. Mater. Chem. B*, 2020, **8**, 8050–8060.

6 L. Panzella, G. Gentile, G. D'Errico, N. F. Della Vecchia, M. E. Errico, A. Napolitano, C. Carfagna and M. D'Ischia, *Angew. Chemie*, 2013, **52**, 12684–12687.

7 G. Vitiello, A. Zanfardino, O. Tammaro, M. Di Napoli, M. F. Caso, A. Pezzella, M. Varcamonti, B. Silvestri, G. D'Errico, A. Costantini and G. Luciani, *RSC Adv.*, 2018, **8**, 28275–28283.

8 P. L. McGeer, S. Itagaki, B. E. Boyes and E. G. McGeer, *Neurology*, 1988, **38**, 1285–

1291.

9 H. P. Oliveira, C. F. O. Graeff, C. L. P. S. Zanta, A. C. Galina and P. J. Gonçalves, *J. Mater. Chem.*, 2000, **10**, 371–375.

10 Y. J. Kim, W. Wu, S. Chun, J. F. Whitacre and C. J. Bettinger, *Proc. Natl. Acad. Sci.*, 2013, **110**, 20912–17.

11 R. Xu, A. Gouda, M. F. Caso, F. Soavi and C. Santato, *ACS Omega*, 2019, **4**, 12244–12251.

12 A. Gouda, S. R. Bobbara, M. Reali and C. Santato, *J. Phys. D. Appl. Phys.*, 2020, **53**, 043003.

13 M. I. N. da Silva, S. N. Dezidério, J. C. Gonzalez, C. F. O. Graeff and M. A. Cotta, *J. Appl. Phys.*, 2004, **96**, 5803–5807.

14 M. Ambrico, P. F. Ambrico, A. Cardone, T. Ligonzo, S. R. Cicco, R. Di Mundo, V. Augelli and G. M. Farinola, *Adv. Mater.*, 2011, **23**, 3332–3336.

15 P. Kumar, E. Di Mauro, S. Zhang, A. Pezzella, F. Soavi, C. Santato and F. Cicoira, *J. Mater. Chem. C*, 2016, **4**, 9516–9525.

16 L. G. S. Albano, J. V. Paulin, L. D. Trino, S. L. Fernandes and C. F. de O. Graeff, *J. Appl. Polym. Sci.*, 2019, **136**, 47805.

17 S. Adhikari, R. A. A. Hopson, B. R. Sedai, F. M. McFarland, S. Guo and T. L. Nelson, *J. Polym. Sci. Part A Polym. Chem.*, 2017, **55**, 457–463.

18 L. Chang, F. Chen, X. Zhang, T. Kuang, M. Li, J. Hu, J. Shi, L. J. Lee, H. Cheng and Y. Li, *ACS Appl. Mater. Interfaces*, 2017, **9**, 16553–16560.

19 L. Migliaccio, S. Aprano, L. Iannuzzi, M. G. Maglione, P. Tassini, C. Minarini, P. Manini and A. Pezzella, *Adv. Electron. Mater.*, 2017, **3**, 1600342.

20 M. Ambrico, A. Cardone, T. Ligonzo, V. Augelli, P. F. Ambrico, S. Cicco, G. M. Farinola, M. Filannino, G. Perna and V. Capozzi, *Org. Electron.*, 2010, **11**, 1809–1814.

21 M. Ambrico, P. F. Ambrico, T. Ligonzo, A. Cardone, S. R. Cicco, A. Lavizzera, V. Augelli and G. M. Farinola, *Appl. Phys. Lett.*, 2012, **100**, 253702.

22 E. Di Mauro, O. Carpentier, S. I. Yáñez Sánchez, N. Ignoumba Ignoumba, M. Lalancette-Jean, J. Lefebvre, S. Zhang, C. F. O. Graeff, F. Cicoira and C. Santato, *J. Mater. Chem. C*, 2016, **4**, 9544–9553.

23 T. Chen, C. Ji, Y. Jin, J. Wang and Q. Jin, *Macromol. Mater. Eng.*, 2018, **303**, 1800319.

24 L. Migliaccio, M. Gryszel, V. Derek, A. Pezzella and E. D. Głowacki, *Mater. Horizons*,

2018, **5**, 984–990.

25 E. Pinna, C. Melis, A. Antidormi, R. Cardia, E. Sechi, G. Cappellini, M. D'Ischia, L. Colombo and G. Mula, *Int. J. Mol. Sci.*, 2017, **18**, 1567.

26 M. V. Tholl, H. G. Akarçay, H. Tanner, T. Niederhauser, A. Zurbuchen, M. Frenz and A. Haeberlin, *Appl. Energy*, 2020, **269**, 114948.

27 M. Piacenti-Silva, J. C. Fernandes, N. B. de Figueiredo, M. Congiu, M. Mulato and C. F. de O. Graeff, *AIP Adv.*, 2014, **4**, 037120.

28 A. Pezzella, M. Barra, A. Musto, A. Navarra, M. Alfè, P. Manini, S. Parisi, A. Cassinese, V. Criscuolo and M. D'Ischia, *Mater. Horizons*, 2015, **2**, 212–220.

29 M. Sheliakina, A. B. Mostert and P. Meredith, *Mater. Horizons*, 2018, **5**, 256–263.

30 Z. Tehrani, S. P. Whelan, B. Mostert, J. V. Paulin, M. M. Ali, E. D. Ahmadi, C. F. de O. Graeff, O. J. Guy and D. T. Gethin, *2D Mater.*, 2020, **7**, 024008.

31 J. P. Bothma, J. de Boor, U. Divakar, P. E. Schwenn and P. Meredith, *Adv. Mater.*, 2008, **20**, 3539–3542.

32 S. N. Dezidério, C. A. Brunello, M. I. N. da Silva, M. A. Cotta and C. F. O. Graeff, *J. Non. Cryst. Solids*, 2004, **338**–**340**, 634–638.

33 M. Piacenti-Silva, E. S. Bronze-Uhle, J. V. Paulin and C. F. O. Graeff, *J. Mol. Struct.*, 2014, **1056**–**1057**, 135–140.

34 K. J. Lawrie, P. Meredith and R. P. McGeary, *Photochem. Photobiol.*, 2008, **84**, 632–638.

35 A. Pezzella, A. Iadonisi, S. Valerio, L. Panzella, A. Napolitano, M. Adinolfi and M. D'Ischia, *J. Am. Chem. Soc.*, 2009, **131**, 15270–5.

36 S. R. Cicco, M. Ambrico, P. F. Ambrico, M. M. Talamo, A. Cardone, T. Ligonzo, R. Di Mundo, C. Giannini, T. Sibillano, G. M. Farinola, P. Manini, A. Napolitano, V. Criscuolo and M. D'Ischia, *J. Mater. Chem. C*, 2015, **3**, 2810–2816.

37 E. S. Bronze-Uhle, J. V. Paulin, M. Piacenti-Silva, C. Battocchio, M. L. M. Rocco and C. F. de O. Graeff, *Polym. Int.*, 2016, **65**, 1339–1346.

38 J. V. Paulin, A. G. Veiga, Y. Garcia-Basabe, M. L. M. Rocco and C. F. Graeff, *Polym. Int.*, 2018, **67**, 550–556.

39 M. Piacenti-Silva, A. A. Matos, J. V. Paulin, R. A. da S. Alavarce, R. C. de Oliveira and C. F. Graeff, *Polym. Int.*, 2016, **65**, 1347–1354.

40 L. G. S. Albano, E. Di Mauro, P. Kumar, F. Cicoira, C. F. O. Graeff and C. Santato, *Polym. Int.*, 2016, **65**, 1315–1322.

41 J. V. Paulin, A. Batagin-Neto, P. Meredith, C. F. O. Graeff and A. B. Mostert, *J. Phys. Chem. B*, 2020, **124**, 10365–10373.

42 J. Wünsche, F. Cicoira, C. F. O. Graeff and C. Santato, *J. Mater. Chem. B*, 2013, **1**, 3836–3842.

43 M. d'Ischia, A. Napolitano, A. Pezzella, P. Meredith and M. J. Buehler, *Angew. Chemie Int. Ed.*, 2020, **59**, 11196–11205.

44 A. B. Mostert, B. J. Powell, F. L. Pratt, G. R. Hanson, T. Sarna, I. R. Gentle and P. Meredith, *Proc. Natl. Acad. Sci. U. S. A.*, 2012, **109**, 8943–7.

45 A. B. Mostert, S. B. Rienecker, C. Noble, G. R. Hanson and P. Meredith, *Sci. Adv.*, 2018, **4**, eaaq1293.

46 M. M. Jastrzebska, H. Isotalo, J. Paloheimo and H. Stubb, *J. Biomater. Sci. Polym. Ed.*, 1995, **7**, 577–586.

47 B. Mostert, B. J. Powell, I. R. Gentle and P. Meredith, *Appl. Phys. Lett.*, 2012, **100**, 093701.

48 J. Wünsche, Y. Deng, P. Kumar, E. Di Mauro, E. Josberger, J. Sayago, A. Pezzella, F. Soavi, F. Cicoira, M. Rolandi and C. Santato, *Chem. Mater.*, 2015, **27**, 436–442.

49 M. Sheliakina, A. B. Mostert and P. Meredith, *Adv. Funct. Mater.*, 2018, **28**, 1805514.

50 M. Reali, P. Saini and C. Santato, *Mater. Adv.*, 2021, **2**, 15–31.

51 E. S. Bronze-Uhle, A. Batagin-Neto, P. H. P. Xavier, N. I. Fernandes and C. F. O. Graeff, *J. Mol. Struct.*, 2013, **1047**, 102–108.

52 B. A. Gilchrest, M. S. Eller, A. C. Geller and M. Yaar, *N. Engl. J. Med.*, 1999, **340**, 1341–1348.

53 B. Owens, *NatureOutlook*, 2014, **515**, S109.

54 E. S. Krol and D. C. Liebler, *Chem. Res. Toxicol.*, 1998, **11**, 1434–1440.

55 T. Repenko, A. Rix, A. Nedilko, J. Rose, A. Hermann, R. Vinokur, S. Moli, R. Cao-Milàn, M. Mayer, G. von Plessen, A. Fery, L. De Laporte, W. Lederle, D. N. Chigrin and A. J. C. Kuehne, *Adv. Funct. Mater.*, 2018, **28**, 1705607.

56 K. A. Motovilov, V. Grinenko, M. Savinov, Z. V. Gagkaeva, L. S. Kadyrov, A. A. Pronin, Z. V. Bedran, E. S. Zhukova, A. B. Mostert and B. P. Gorshunov, *RSC Adv.*, 2019, **9**, 3857–3867.

57 S. B. Rienecker, A. B. Mostert, G. Schenk, G. R. Hanson and P. Meredith, *J. Phys. Chem. B*, 2015, **119**, 14994–15000.

58 J. V. Paulin, J. D. Mcgettrick, C. F. O. Graeff and A. B. Mostert, *Surf. Interface*, 2021, **24**, 101053.

59 G. Schaftenaar and J. H. Noordik, *J. Comput. Aided. Mol. Des.*, 2000, **14**, 123–134.

60 J. J. P. Stewart, MOPAC2016, http://openmopac.net/MOPAC2016.html.

61 A. D. Becke, *J. Chem. Phys.*, 1993, **98**, 5648–5652.

62 M. J. Frisch, G. W. Trucks, H. B. Schlegel, G. E. Scuseria, M. Robb, J. Cheeseman, G. Scalmani, V. Barone, B. Mennucci, G. A. H. Petersson, H. Nakatsuji, M. Caricato, X. Li, H. P. Hratchian, A. F. Izmaylov, J. Bloino, G. Zheng, J. L. Sonnenberg, M. Hada and D. Fox, 2009.

63 C. Haichuan, J. Guozhu, Z. Liang and H. Yinshu, *Phys. Chem. Liq.*, 2014, **53**, 435–442.

64 C. L. Serpentini, C. Gauchet, D. De Montauzon, M. Comtat, J. Ginestar and N. Paillous, *Electrochim. Acta*, 2000, **45**, 1663–1668.

65 D. Nečas and P. Klapetek, *Cent. Eur. J. Phys.*, 2012, **10**, 181–188.

66 R. Kerremans, C. Kaiser, W. Li, N. Zarrabi, P. Meredith and A. Armin, *Adv. Opt. Mater.*, 2020, **8**, 2000319.

67 D. Tuna, A. Udvarhelyi, A. L. Sobolewski, W. Domcke and T. Domratcheva, *J. Phys. Chem. B*, 2016, **120**, 3493–3502.

68 J. B. Nofsinger, E. E. Weinert and J. D. Simon, *Biopolymers*, 2002, **67**, 302–305.

69 G. S. Lorite, V. R. Coluci, M. I. N. da Silva, S. N. Dezidério, C. F. O. Graeff, D. S. Galvão and M. Cotta, *J. Appl. Phys.*, 2006, **99**, 113511-1/113511-6.

70 W. Li, A. Patil, X. Zhou, Z. Wang, M. Xiao, M. D. Shawkey, N. C. Gianneschi and A. Dhinojwala, *Appl. Phys. Lett.*, 2020, **117**, 203701.

71 D. G. Stavenga, H. L. Leertouwer, D. C. Osorio and B. D. Wilts, *Light Sci. Appl.*, 2015, **4**, e243.

72 J. G. Liu and M. Ueda, *J. Mater. Chem.*, 2009, **19**, 8907–8919.

73 T. S. Kleine, R. S. Glass, D. L. Lichtenberger, M. E. Mackay, K. Char, R. A. Norwood and J. Pyun, *ACS Macro Lett.*, 2020, **9**, 245–259.

74 T. Higashihara and M. Ueda, *Macromolecules*, 2015, **48**, 1915–1929.

75 J. G. Liu, Y. Nakamura, Y. Suzuki, Y. Shibasaki, S. Ando and M. Ueda, *Macromolecules*, 2007, **40**, 7902–7909.

76 L. Glasser, *Chem. Rev.*, 1975, **75**, 21–65.

77 R. A. Huggins, *Ionics (Kiel).*, 2002, **8**, 300–313.

78 E. P. Randviir and C. E. Banks, *Anal. Methods*, 2013, **5**, 1098–1115.

79 J. Bisquert, G. Garcia-Belmonte, P. Bueno, E. Longo and L. O. S. Bulhões, *J. Electroanal. Chem.*, 1998, **452**, 229–234.

80 F. Bernsmann, J.-C. Voegel and V. Ball, *Electrochim. Acta*, 2011, **56**, 3914–3919.

81 V. Gargiulo, M. Alfè, R. Di Capua, A. R. Togna, V. Cammisotto, S. Fiorito, A. Musto, A. Navarra, S. Parisi and A. Pezzella, *J. Mater. Chem. B*, 2015, **3**, 5070–5079.

82 M. Ambrico, P. F. Ambrico, T. Ligonzo, A. Cardone, M. G. Bridelli, G. Casamassima, P. Manini and M. D'Ischia, *Phys. Chem. Chem. Phys.*, 2017, **19**, 9432–9443.

83 J. Bisquert and A. Compte, *J. Electroanal. Chem.*, 2001, **499**, 112–120.

84 J. Bisquert, *J. Phys. Chem. B*, 2002, **106**, 325–333.

85 I. S. Kwon, Y. J. Kim, L. Klosterman, M. Forssell, G. K. Fedder and C. J. Bettinger, *Jounal Mater. Chem. B*, 2016, **4**, 3031–3036.

86 T. Soboleva, Z. Xie, Z. Shi, E. Tsang, T. Navessin and S. Holdcroft, *J. Electroanal. Chem.*, 2008, **622**, 145–152.

87 D. D. Ordinario, L. Phan, W. G. Walkup Iv, J.-M. Jocson, E. Karshalev, N. Hüsken and A. A. Gorodetsky, *Nat. Chem.*, 2014, **6**, 596–602.

88 L. M. Almeida, J. F. Floriano, T. P. Ribeiro, L. N. Magno, L. S. L. S. Da Mota, N. Peixoto, F. Mrué, P. Melo-Reis, R. D. S. Lino, C. F. D. O. Graeff and P. J. Gonçalves, *J. Mater. Sci. Mater. Med.*, 2014, **25**, 2153–2162.

89 Y. van de Burgt, E. Lubberman, E. J. Fuller, S. T. Keene, G. C. Faria, S. Agarwal, M. J. Marinella, A. Alec Talin and A. Salleo, *Nat. Mater.*, 2017, **16**, 414–418.